Available online at www.sciencedirect.com
ScienceDirect
Computers & Fluids 36 (2007) 12–26
computers & fluids
www.elsevier.com/locate/compfluid

Weak imposition of Dirichlet boundary conditions in fluid mechanics

Y. Bazilevs, T.J.R. Hughes *

Institute for Computational Engineering and Sciences, The University of Texas at Austin, 201 East 24th Street, 1 University Station C0200, Austin, TX 78712, USA

Received 29 June 2005; accepted 15 July 2005
Available online 2 December 2005

Abstract

Weakly enforced Dirichlet boundary conditions are compared with strongly enforced conditions for boundary layer solutions of the advection–diffusion equation and incompressible Navier–Stokes equations. It is found that weakly enforced conditions are effective and superior to strongly enforced conditions. The numerical tests involve low-order finite elements and a quadratic NURBS basis utilized in the Isogeometric Analysis approach. The convergence of the mean velocity profile for a turbulent channel flow suggests that weak no-slip conditions behave very much like a wall function model, although the design of the boundary condition is based purely on numerical, rather than physical or empirical, conditions.

1. Introduction

Dirichlet boundary condition specification in computational fluid dynamics, such as the no-slip wall boundary condition for the Navier–Stokes equations, is rarely discussed. It seems so simple and unambiguous. Just set the variables to their prescribed values. But what precisely does that mean? In formulations in which continuous representations of the fields are employed, such as traditional finite element methods employing C^0 nodal interpolations, the nodal values are specified. This amounts to so-called "strong satisfaction" of the boundary conditions. "Strong" sounds good but certain deficiencies may arise. For example, if the boundary data is discontinuous, C^0 interpolation with higher-order Lagrange polynomial finite elements will result in oscillations rather than a crisp resolution of the data. In addition, it has been repeatedly noted over the years that strongly enforced outflow boundary conditions give rise to spurious oscillations even for methods with otherwise good stability properties. So maybe strong satisfaction is not such a good idea. What is the alternative? There is the possibility of "weak satisfaction" in which the functions representing the discrete solution are not required to satisfy the Dirichlet conditions but rather terms are added to the variational equations to enforce them weakly as Euler–Lagrange conditions. A methodology which does this is the discontinuous Galerkin (DG) method in which discontinuous solution spaces are employed and all continuity and boundary conditions are satisfied weakly. The DG method has its strengths and weaknesses but these will not be discussed here. See [1,2,4,6,10,15,18,22,26,34,40,42,44,45,50,53] for recent works on the DG method. Despite the large and growing literature on the DG method, we are not aware of any study comparing the weak satisfaction of Dirichlet conditions with more traditional and common strong satisfaction. It is the purpose of this paper to perform a comparison in the context of stabilized, continuous Galerkin (CG) finite element formulations of the

* Corresponding author. Tel.: +1 512 232 7775; fax: +1 512 232 7508.
E-mail address: tjr_hughes@hotmail.com (T.J.R. Hughes).

0045-7930/$ - see front matter © 2005 Elsevier Ltd. All rights reserved.
doi:10.1016/j.compfluid.2005.07.012

advection–diffusion equation and incompressible Navier–Stokes equations.

In Section 2 we describe the strong and weak formulations of the continuous problem for the advection–diffusion equation, and a stabilized Galerkin method with weakly enforced Dirichlet boundary conditions. We also describe a method to accurately calculate the diffusive flux which attains conservation. Numerical tests are performed in Section 3 for boundary layer problems in one, two and three dimensions. Linear and bilinear finite elements are used in the one- and two-dimensional examples, and quadratic NURBS are used in the three-dimensional case. In the latter case, we are able to constructs an exact geometric model of a hollow cylinder through the use of the Isogeometric Analysis approach [32]. The weak Dirichlet boundary conditions perform well and are able to mitigate or entirely eliminate oscillations about unresolved boundary layers. This also appears to improve the accuracy in the domain away from the layers. In Section 4 we describe the stabilized formulation for the incompressible Navier–Stokes equations. We compare strong and weak treatment of no-slip boundary conditions. In both cases we strongly satisfy the wall-normal velocity boundary condition. As a basis for comparison, we consider an equilibrium turbulent channel flow at a friction-velocity Reynolds number of 180 simulated with trilinear hexahedral finite elements. Based on mean velocity profiles, we conclude that weak no-slip boundary conditions provide significant increases in accuracy over strong for coarse meshes. For fine meshes, results converge toward the DNS benchmark solution of Kim et al. [37]. It is noted that the approach utilized may be viewed as somewhere between a coarse DNS and an LES in that the stabilization terms model the cross-stress contributions to energy transfer. Nevertheless, a surprisingly good result is obtained for a medium mesh with weakly enforced no-slip boundary conditions. It seems weak enforcement behaves somewhat like a wall function model although no turbulence physics or empiricism is incorporated in its design. In Section 5 we draw conclusions.

2. The advection–diffusion equation

2.1. Strong and weak formulations of the continuous problem

Let Ω be an open, connected, bounded subset of $\mathbb{R}^d$, $d = 2$ or 3, with piecewise smooth boundary $\Gamma = \partial\Omega$. Ω represents the fixed spatial domain of the problem. Let $f : \Omega \to \mathbb{R}$ be the given source; $\boldsymbol{a} : \Omega \to \mathbb{R}^d$ is the spatially varying velocity vector, assumed solenoidal; $\boldsymbol{\kappa} : \Omega \to \mathbb{R}^{d\times d}$ is the diffusivity tensor, assumed symmetric, positive-definite; and $g : \Gamma \to \mathbb{R}$ is the prescribed Dirichlet boundary data. Let Γ_{in} be a subset of Γ on which $\boldsymbol{a}\cdot\boldsymbol{n} < 0$ and $\Gamma_{\text{out}} = \Gamma - \Gamma_{\text{in}}$, the inflow and the outflow boundary, respectively. The boundary value problem consists of solving the following equations for $u : \overline{\Omega} \to \mathbb{R}$:

$$\mathscr{L}u = f \quad \text{in } \Omega, \tag{1}$$

$$u = g \quad \text{on } \Gamma, \tag{2}$$

where

$$\mathscr{L}u = \nabla\cdot(\boldsymbol{a}u) - \nabla\cdot(\boldsymbol{\kappa}\nabla u) = \boldsymbol{a}\cdot\nabla u - \nabla\cdot(\boldsymbol{\kappa}\nabla u), \tag{3}$$

the last equality holding true due to the divergence-free condition on the velocity field. Defining the solution and the weighting spaces as

$$H^1_g(\Omega) = \{u \mid u \in H^1(\Omega), u = g \text{ on } \Gamma\}, \tag{4}$$

$$H^1_0(\Omega) = \{u \mid u \in H^1(\Omega), u = 0 \text{ on } \Gamma\}, \tag{5}$$

respectively, the variational counterpart of (1) is

find $u \in H^1_g(\Omega)$ such that $\forall w \in H^1_0(\Omega)$,

$$(-\nabla w, \boldsymbol{a}u - \boldsymbol{\kappa}\nabla u)_\Omega - (w, f)_\Omega = 0, \tag{6}$$

where $(\cdot,\cdot)_\Omega$ denotes the L^2-inner product on Ω.

Remark. For simplicity of exposition we consider all of Γ to be the Dirichlet boundary. The methods presented herein extend in a straightforward fashion to cases where other boundary conditions are prescribed on parts of Γ.

2.2. Finite element formulation of the advection–diffusion equation with Dirichlet boundary conditions imposed weakly

Consider a finite element partition of the physical domain Ω into n_{el} elements

$$\Omega = \bigcup_e \Omega_e, \quad e = 1, \ldots, n_{el}, \tag{7}$$

which induces a partition of the boundary into n_{eb} segments as

$$\Gamma = \bigcup_b \Gamma_b \cap \Gamma, \quad b = 1, \ldots, n_{eb}. \tag{8}$$

Typical finite element approximation spaces are subspaces of

$$\mathscr{V}^h = \{u \mid u \in C^k(\Omega) \cap \mathscr{P}^l(\Omega_e)\ \forall e = 1, \ldots, n_{el}\}, \tag{9}$$

where k is the degree of continuity of the functions on interelement boundaries and l is the polynomial order of the functions on element interiors. In most cases, $k = 0$ and $l = 1$, namely a piecewise linear, C^0-continuous basis is employed. It is standard practice to impose Dirichlet boundary conditions strongly. That is, the finite element trial solution and weighting spaces are required to be subsets of (4) and (5), respectively. In this work, no such constraints are imposed on $\mathscr{V}^h$, instead

Dirichlet boundary conditions are built into the variational formulation weakly, as described in what follows.

Remark. For all but one case considered in this paper, the polynomial order of the basis functions is equal to one. The exception is an application of the Isogeometric Analysis approach proposed by Hughes et al. [32].

Given the approximation space $\mathscr{V}^h$, our method is stated as follows:

Find $u^h \in \mathscr{V}^h$ such that $\forall w^h \in \mathscr{V}^h$,

$$\begin{aligned}
&(-\nabla w^h, \boldsymbol{a}u^h - \boldsymbol{\kappa}\nabla u^h)_\Omega - (w^h, f)_\Omega + \sum_{e=1}^{n_{el}} (\mathbb{L}w^h\tau, \mathscr{L}u^h - f)_{\Omega_e} \\
&+ \sum_{b=1}^{n_{eb}} (w^h, -\boldsymbol{\kappa}\nabla u^h \cdot \boldsymbol{n} + \boldsymbol{a}\cdot\boldsymbol{n}u^h)_{\Gamma_b\cap\Gamma} \\
&+ \sum_{b=1}^{n_{eb}} (-\gamma\boldsymbol{\kappa}\nabla w^h \cdot \boldsymbol{n} - \boldsymbol{a}\cdot\boldsymbol{n}w^h, u^h - g)_{\Gamma_b\cap\Gamma_{\text{in}}} \\
&+ \sum_{b=1}^{n_{eb}} (-\gamma\boldsymbol{\kappa}\nabla w^h \cdot \boldsymbol{n}, u^h - g)_{\Gamma_b\cap\Gamma_{\text{out}}} \\
&+ \sum_{b=1}^{n_{eb}} \left(\frac{C_b^I|\boldsymbol{\kappa}|}{h_b} w^h, u^h - g\right)_{\Gamma_b\cap\Gamma} = 0,
\end{aligned} \tag{10}$$

where $\boldsymbol{n}$ is the unit outward normal vector to Γ, $(\cdot,\cdot)_{\mathscr{D}}$ defines the L^2-inner product on $\mathscr{D} = \Omega$, Ω_e, etc., and γ and C_b^I are non-dimensional constants.

Remarks

(1) The stabilized methods SUPG, GLS and MS are obtained by appropriate selection of $\mathbb{L}$. See Hughes et al. [30] for elaboration. The intrinsic element time scale, τ, is also described in [30] and references therein. In the numerical calculations, we use SUPG in which

$$\mathbb{L}w^h = \boldsymbol{a}\cdot\nabla w^h. \tag{11}$$

The definition of the intrinsic time scale is taken to be

$$\tau = \frac{h_{\boldsymbol{a}}}{2|\boldsymbol{a}|}\min\left(1, \frac{1}{3p^2}Pe\right), \tag{12}$$

where Pe, the element Peclet number, is defined as

$$Pe = \frac{|\boldsymbol{a}|h_{\boldsymbol{a}}}{2|\boldsymbol{\kappa}|}, \tag{13}$$

$h_{\boldsymbol{a}}$ is the element size in the direction of the flow, and p is the polynomial order of the basis. For a summary of the early literature on SUPG see Brooks and Hughes [12]. Recent work on stabilized methods is presented in [3,8,9,13,19–21,23,24,38,41,48]. Construction of the intrinsic time scale τ, given by (12), is based on the single advective length scale, $h_{\boldsymbol{a}}$. It appears sufficient for the type of test cases considered in this paper. More sophisticated definitions of τ based on multiple element length scales are given in Tezduyar [49]. These intrinsic time scales exhibit superior robustness in calculations of industrial size and complexity, and it is our intent to use them in the future work on weak imposition of Dirichlet boundary conditions.

(2) The fourth term of (10) is the so-called *consistency* term. In obtaining the Euler–Lagrange equations corresponding to (10), integration-by-parts produces a term that is cancelled by the consistency term. The remaining terms are precisely the desired ones, namely, the weak form of the advection–diffusion equation and appropriate boundary conditions.

(3) The last three terms of (10) are responsible for the enforcement of the Dirichlet boundary conditions. Note the difference in the treatment of inflow and outflow boundaries. As long as some diffusion is present, it is permissible to set Dirichlet boundary conditions on the entire domain boundary Γ. On the other hand, in the case of no diffusion, one can only set the values of the solution on the inflow part of the boundary, namely Γ_{in}. Hence, our treatment of outflow and inflow is different. We make both advection and diffusion responsible for enforcing the inflow Dirichlet boundary conditions by including advective and diffusive parts of the total flux operator acting on the weighting function w^h. The outflow boundary integral only sees the diffusive part of the total flux operator acting on w^h. The mathematical structure of these terms puts more weight on the Dirichlet boundary condition at the inflow than at the outflow in the advection dominated case. In addition, it forces the outflow Dirichlet boundary condition to vanish in the advective limit. Note that, in the limit of zero diffusion, a correct discrete variational formulation for pure advection is obtained.

(4) In this work, we assume $\gamma = 1$ or -1. Both choices yield consistent methods. At first glance, one might consider $\gamma = -1$ a better choice because it leads to better stability of the bilinear form when diffusion is significant. Unfortunately, this renders the formulation *adjoint-inconsistent*, which, in turn, may lead to suboptimal convergence in lower-order norms, such as L^2 (see Arnold et al. [5]). There is some evidence of this in our first numerical example. In addition, $\gamma = -1$ produces non-monotone behavior in boundary layers where advection is non-negligible. It is worth noting that solutions for $\gamma = 1$, the adjoint-consistent case, are monotone for all discretizations and converge at optimal rate in L^2. The last term in (10) is penalty-like. It renders the formulation non-singular in the absence of advection as well as produces a stabilizing effect necessary for the $\gamma = 1$ case. The inverse power of h is necessary for optimal rate of convergence. The element-wise

constant C_b^I is not arbitrary. For the $\gamma = 1$ case, C_b^I has to be greater than some $\tilde{C}$ which, in turn, comes from the local boundary inverse estimate

$$\|\nabla w^h \cdot \boldsymbol{n}\|_{L^2(\Gamma_b)} \leqslant \frac{\tilde{C}}{2h_b}\|w^h\|_{L^2(\Gamma_b)} \quad \forall w^h \in \mathscr{V}^h. \tag{14}$$

$\tilde{C}$ is dependent on the order of interpolation used and the element type (see Ciarlet [17]), and is, in principle, computable for any discretization. For the case when $\gamma = -1$, C_b^I just has to be strictly greater than zero to ensure stability. Note also that the last term in (10) scales with $\boldsymbol{\kappa}$, which means that it becomes less important when advection dominates and vanishes completely in the advective limit.

(5) One can obtain formulation (10), without interior stabilization (i.e., the $\mathbb{L}$ term), from a variety of discontinuous Galerkin (DG) methods. For example, the case of $\gamma = -1, C_b^I = 0$ corresponds to the method of Baumann and Oden [7]; $\gamma = -1$, $C_{eb}^I > 0$ is the non-symmetric interior penalty Galerkin (NIPG) method [43]; and $\gamma = -1$, $C_{eb}^I > 0$ is the symmetric interior penalty Galerkin (SIPG) method [51].

2.3. Computation of the diffusive flux

Diffusive flux, namely

$$q^{\text{diff}} = \boldsymbol{\kappa}\nabla u \cdot \boldsymbol{n}, \tag{15}$$

is a very important quantity in engineering analysis. In the presence of unresolved boundary layers, a direct evaluation of the normal gradient of the discrete solution, as suggested by the above definition, generally leads to inaccurate results. In this section we give a definition of the diffusive flux which is based on the idea of global conservation (see Hughes et al. [33] and Brezzi, Hughes, and Süli [11] for background). The structure of formulation (10) is such that no additional processing needs to be done to determine a conserved quantity.

We restate the boundary value problem (6) as follows (see Hughes et al. [33]): find $u \in H_g^1(\Omega)$, $q \in H^{-1/2}(\Gamma)$ such that $\forall w \in H^1(\Omega)$,

$$(-\nabla w, \boldsymbol{a}u - \boldsymbol{\kappa}\nabla u)_\Omega - \langle w, q\rangle_\Gamma - (w, f)_\Omega = 0, \tag{16}$$

where $\langle\cdot,\cdot\rangle_\Gamma$ denotes a duality pairing between $H^{1/2}(\Gamma)$ and $H^{-1/2}(\Gamma)$. Let $B(\Omega)$ be a complement of $H_0^1(\Omega)$ in the space $H^1(\Omega)$. Then problem (16) splits into

$$(-\nabla w_0, \boldsymbol{a}u - \boldsymbol{\kappa}\nabla u)_\Omega - (w_0, f)_\Omega = 0 \quad \forall w_0 \in H_0^1(\Omega) \tag{17}$$

and

$$(-\nabla w_b, \boldsymbol{a}u - \boldsymbol{\kappa}\nabla u)_\Omega - \langle w_b, q\rangle_\Gamma - (w_b, f)_\Omega = 0 \quad \forall w_b \in B(\Omega). \tag{18}$$

Applying Green's Identity to (18) and using the fact that (1) holds in $L^2(\Omega)$ (apply standard distribution theory arguments to (17)) yields:

$$-\langle w_b, \boldsymbol{a}\cdot\boldsymbol{n}u - \boldsymbol{\kappa}\nabla u\cdot\boldsymbol{n}\rangle_\Gamma - \langle w_b, q\rangle_\Gamma = 0 \quad \forall w_b \in B(\Omega), \tag{19}$$

which, in turn, implies

$$q = \boldsymbol{\kappa}\nabla u\cdot\boldsymbol{n} - \boldsymbol{a}\cdot\boldsymbol{n}u \quad \text{in } H^{-1/2}(\Gamma). \tag{20}$$

Setting $w = 1$ in (16) also shows that q is globally conservative, that is,

$$-(1, f)_\Omega - (1, q)_\Gamma = 0. \tag{21}$$

Relation (21) implies that whatever is generated in the interior of the domain Ω by the source f is taken out through its boundary Γ by the flux q. The flux q is composed of two parts, q^{adv} and q^{diff}, the advective and diffusive fluxes. The advective flux is prescribed through the Dirichlet boundary condition (i.e., $u = g$ on Γ implies $q^{\text{adv}} = -\boldsymbol{a}\cdot\boldsymbol{n}g$ on Γ). We proceed by defining q^{diff} as

$$q^{\text{diff}} = q - q^{\text{adv}} = q + \boldsymbol{a}\cdot\boldsymbol{n}g \quad \text{on } \Gamma. \tag{22}$$

Remark. Note that our definition coincides with the conventional one, namely (15), but we arrive at it using conservation ideas. The diffusive flux is viewed as the difference between the quantity which is globally conservative and the quantity which is exact. This idea proves very useful in the discrete setting.

We treat the discrete case analogously. Introducing $w^h = 1$ into (10) yields the following discrete conservation law:

$$\begin{aligned} &-(1, f) + \sum_{b=1}^{n_{eb}} (1, (C_b^I|\boldsymbol{\kappa}|/h_b)(u^h - g))_{\Gamma_b} \\ &- \sum_{b=1}^{n_{eb}} (1, \boldsymbol{\kappa}\nabla u^h\cdot\boldsymbol{n} - \boldsymbol{a}\cdot\boldsymbol{n}g)_{\Gamma_b\cap\Gamma_{\text{in}}} \\ &- \sum_{b=1}^{n_{eb}} (1, \boldsymbol{\kappa}\nabla u^h\cdot\boldsymbol{n} - \boldsymbol{a}\cdot\boldsymbol{n}u^h)_{\Gamma_b\cap\Gamma_{\text{out}}} = 0, \end{aligned} \tag{23}$$

where the last three terms represent the globally conserved total flux. Applying definition (22) gives a globally conservative diffusive flux in the discrete setting:

$$\begin{aligned} q^{\text{diff}} &= \boldsymbol{\kappa}\nabla u^h\cdot\boldsymbol{n} - (C_b^I|\boldsymbol{\kappa}|/h_b)(u^h - g) \quad \text{on } \Gamma_{\text{in}}\cap\Gamma_b, \\ q^{\text{diff}} &= \boldsymbol{\kappa}\nabla u^h\cdot\boldsymbol{n} - ((C_b^I|\boldsymbol{\kappa}|/h_b) + \boldsymbol{a}\cdot\boldsymbol{n})(u^h - g) \\ &\quad \text{on } \Gamma_{\text{out}}\cap\Gamma_b. \end{aligned} \tag{24}$$

Remarks

(1) Eqs. (24) indicate that the diffusive flux should be computed differently for inflow and outflow boundaries. Both incorporate the error in the Dirichlet boundary condition scaled by the param-

eter $C_b^I|\boldsymbol{\kappa}|/h_b$. The expression for the outflow diffusive flux also incorporates the error in the advective flux. In cases of small diffusion, the latter contribution becomes dominant.

(2) Expressions (24) are well defined on boundary element edges in two dimensions and boundary element faces in three dimensions.

3. Advection–diffusion numerical tests

In the examples, $\boldsymbol{\kappa}$ is isotropic, that is $\boldsymbol{\kappa} = \kappa \boldsymbol{I}$, where $\kappa > 0$ is a scalar diffusivity and $\boldsymbol{I}$ is the identity tensor. In this case $|\boldsymbol{\kappa}| = \kappa$.

3.1. One-dimensional outflow boundary layer

In this example we consider the outflow boundary layer problem posed on a one-dimensional domain of length 1. The advective velocity $a = 1$, which renders $x = 0$ an inflow boundary and $x = 1$ an outflow boundary. The diffusivity κ is 0.01. The boundary conditions are $u(x = 0) = 1$ and $u(x = 1) = 0$, the latter responsible for a thin outflow layer. The problem setup is depicted in Fig. 1.

Both $\gamma = 1$ and $\gamma = -1$ are considered, and $C_b^I = 4$. The solution was computed using uniform meshes of 8, 16, 32, 64, 128, 256, and 512 C^0 piecewise linear finite elements. Fig. 2 shows the comparison between the computed solutions (up to the solution obtained with 128 elements) for $\gamma = 1$ and $\gamma = -1$. The adjoint-inconsistent formulation produces a non-monotone result, while the adjoint-consistent solution is monotone for all discretizations. The latter property is of great importance in many CFD applications. Note that the non-monotone behavior is most pronounced for the 32 element mesh, which corresponds to the element Peclet number of about 1.5. This is a regime in which both advection and diffusion are equally important.

Figs. 3 and 4 show convergence of the error in the H^1 seminorm and L^2 norm, respectively. In contrast with observations about the monotonicity of the computed solution, based on the error plots one might conclude that the $\gamma = -1$ case is performing slightly better, at least on coarser meshes. However, the inability of the adjoint-inconsistent formulation to converge at optimal order in the L^2 norm in the diffusive limit can be seen in Fig. 4.

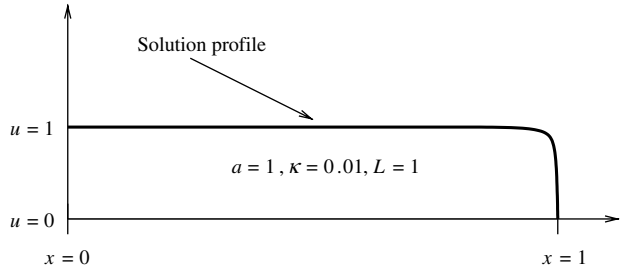

Fig. 1. Setup for a one-dimensional outflow boundary layer problem.

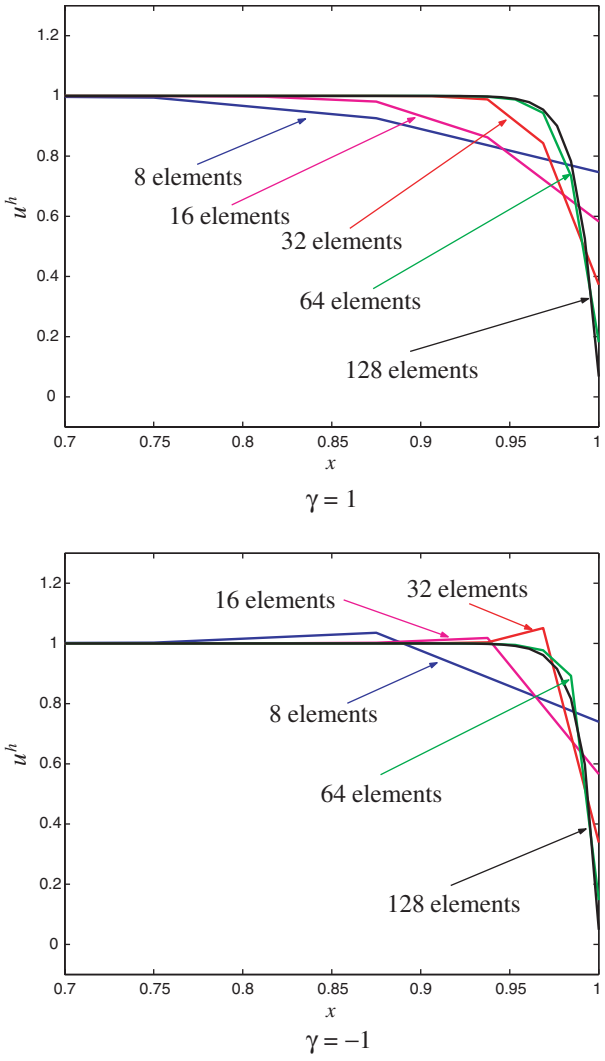

Fig. 2. One-dimensional outflow boundary layer problem. Computed solution profiles. The adjoint-consistent formulation ($\gamma = 1$) gives rise to monotone solutions. The adjoint-inconsistent case ($\gamma = -1$) does not.

3.2. Advection–diffusion in an annular region

This three-dimensional example deals with an advection–diffusion problem posed over an annular region. Problem geometry and parameters are given in Fig. 5. The analytical solution, given here for completeness, varies logarithmically in the radial direction and exponentially in the direction of the flow:

$$u(x, r) = \frac{(e^{ax/\kappa} - e^{aL/\kappa}) \log(r)}{(1 - e^{aL/\kappa}) \log(2)}. \tag{25}$$

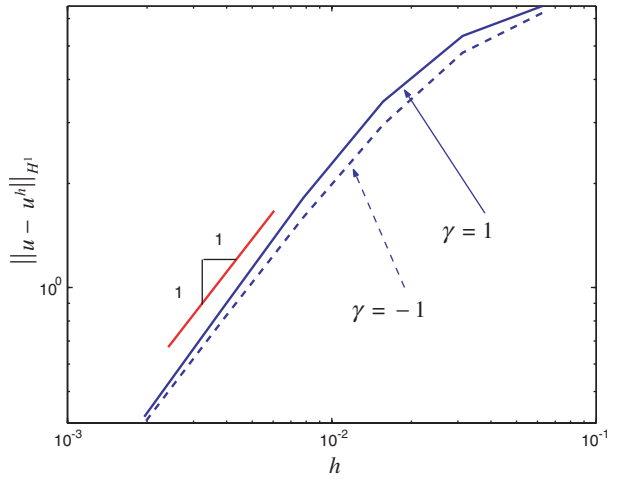

Fig. 3. One-dimensional outflow boundary layer problem. Convergence in the H^1 seminorm.

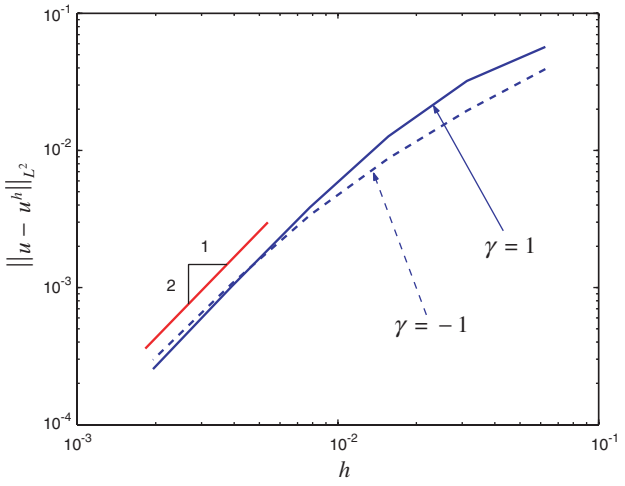

Fig. 4. One-dimensional outflow boundary layer problem. Convergence in the L^2 norm.

In this example (and all subsequent examples in this paper), $\gamma = 1$ was employed. For this case, $C_b^I = 8$. This problem was solved with the Isogeometric Analysis approach proposed by Hughes et al. [32]. Four meshes, composed of 32, 256, 2048 and 16,384 elements were used. The first three are shown in Fig. 6. The meshes are "biased" toward the outflow boundary where there is a thin layer. A quadratic NURBS basis is employed in all three parametric directions enabling us to construct an *exact* isoparametric geometric model. The diffusivity κ, set to 0.025, produces a solution than can be fairly well resolved on meshes 2–4. Axisymmetry was not assumed, yet a pointwise axisymmetric response was obtained in all cases. Figs. 7 and 8 are illustrative. Fig. 9 shows the solution as a function of the axial variable for two fixed values of the radial coordinate, namely $r = 1.5$ and $r = 2.0$. Note the stability of the solution and the degree to which the Dirichlet boundary conditions are satisfied. Finally, the L^2 norm and H^1 seminorm of the error are presented in Fig. 10. Optimal convergence rates are attained.

3.3. Advection skew to the mesh with outflow Dirichlet boundary conditions

The problem setup is given in Fig. 11. The presence of unresolved interior and boundary layers causes difficulties for most existing techniques. Oscillations are typically seen in the vicinities of the layers. In this example, the angle of advection is chosen to be approximately 63.4° so as to avoid any symmetries in the solution with respect to the 20×20 mesh of square bilinear finite elements. $C_b^I = 4$. Fig. 12 shows the SUPG solution obtained with strongly imposed Dirichlet boundary conditions. Very poor behavior is seen at the outflow where the overshoot in the computed solution exceeds 50% of the exact solution. The interior layer is also not perfect but appears to be somewhat under control. Fig. 13 shows the solution for weakly imposed Dirichlet boundary conditions obtained with (10). The inflow boundary condition is captured fairly well but a slight oscillation is observed in the region of the discontinuity. On the other hand, the method completely ignores the outflow Dirichlet boundary condition. This is not surprising, as the degree to which an outflow boundary condition is satisfied depends on the magnitude of the diffusion, which is practically zero in this case. In fact, for such a crude mesh, the problem is almost like pure advection and the method automatically adjusts the boundary conditions accordingly. To avoid oscillations at the inflow, one might choose to set the inflow boundary condition strongly but maintain weak imposition of the outflow Dirichlet boundary condition. This result is shown in Fig. 14, where the solution is very similar to the all-weak case with the exception of the inflow, which is interpolated and thus monotone for linear elements. This device would not work for higher-order finite elements because interpolation creates oscillations. See Hughes et al. [32] for a discussion and an alternative approach utilizing NURBS. Fig. 15 shows a comparison of the all-strong solution with the strong inflow–weak outflow solution in which the prescribed Dirichlet boundary condition is inserted a posteriori (i.e., computed values of the solution were overwritten with their prescribed counterparts). A "perfect" outflow layer for the computational mesh is obtained in this case.

4. Incompressible Navier–Stokes equations

In this section we consider viscous incompressible flow in a bounded domain with no-slip conditions imposed on the boundary. This is the setting for

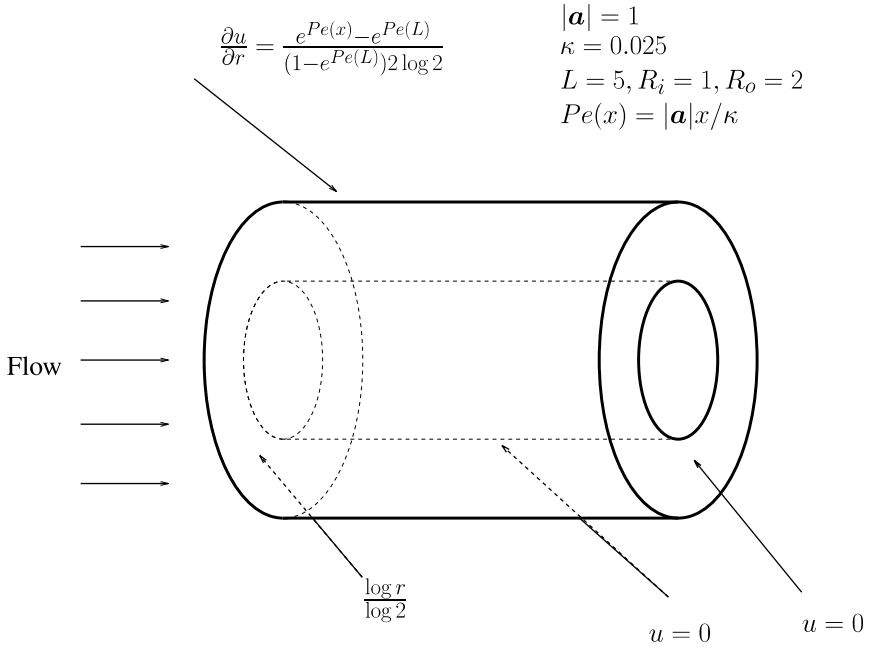

Fig. 5. Advection–diffusion in an annular region. Problem setup.

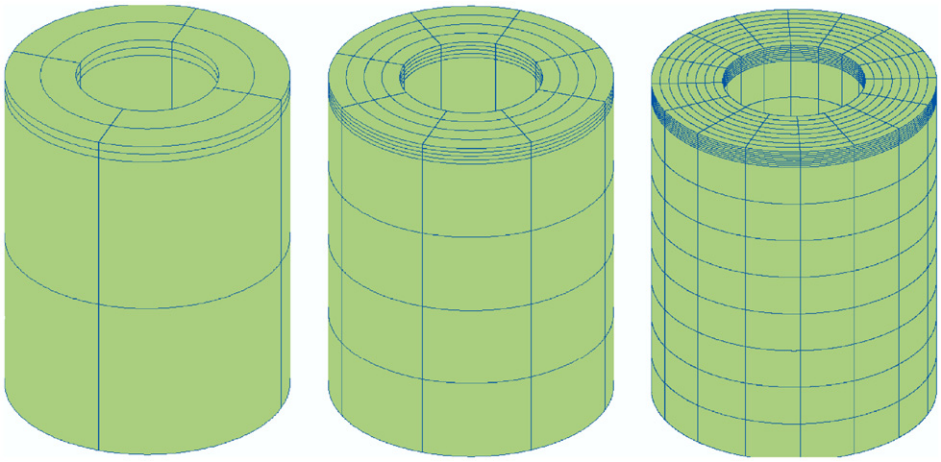

Fig. 6. Advection–diffusion in an annular region. Meshes 1–3.

wall-bounded flows where, in the high Reynolds number regime, turbulent boundary layers occur. In order to accurately solve these flows, one needs to resolve the boundary layers, which is prohibitively expensive. In this work we are hoping to demonstrate that the computational cost associated with boundary layer computations can be reduced, without compromising the accuracy of the solution, by imposing the no-slip condition weakly. The advection–diffusion calculations are an indication that errors associated with under-resolving boundary layers are reduced away from the layers when Dirichlet boundary conditions are imposed weakly. The same observation was made by Layton [39], who examined weak imposition of boundary conditions for the case of the Stokes equations.

We begin by considering a weak formulation of the incompressible Navier–Stokes (INS) equations. Let $\mathscr{V}$ denote the trial solution and weighting function spaces, which are assumed to be same. We also assume $\boldsymbol{u} = \boldsymbol{0}$ on Γ and $\int_\Omega p(t)\,\mathrm{d}\Omega = 0$ for all $t \in]0, T[$. The variational formulation is stated as follows: Find $\boldsymbol{U} = \{\boldsymbol{u}, p\} \in \mathscr{V}$ such that $\forall \boldsymbol{W} = \{\boldsymbol{w}, q\} \in \mathscr{V}$,

$$B(\boldsymbol{W}, \boldsymbol{U}) = (\boldsymbol{W}, \boldsymbol{F}), \tag{26}$$

where

$$B(\boldsymbol{W}, \boldsymbol{U}) = \left(\boldsymbol{w}, \frac{\partial \boldsymbol{u}}{\partial t}\right)_\Omega - (\nabla \boldsymbol{w}, \boldsymbol{u} \otimes \boldsymbol{u})_\Omega + (q, \nabla \cdot \boldsymbol{u})_\Omega - (\nabla \cdot \boldsymbol{w}, p)_\Omega + (\nabla^s \boldsymbol{w}, 2\nu \nabla^s \boldsymbol{u})_\Omega, \tag{27}$$

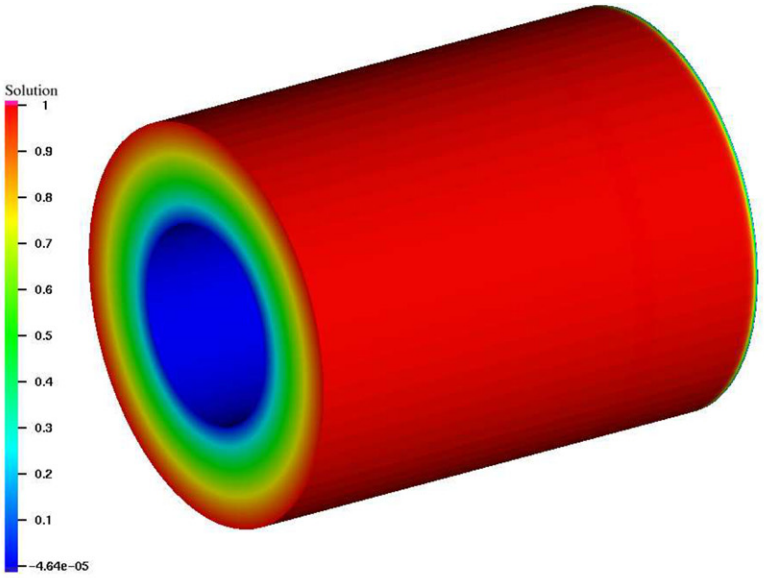

Solution on the whole domain

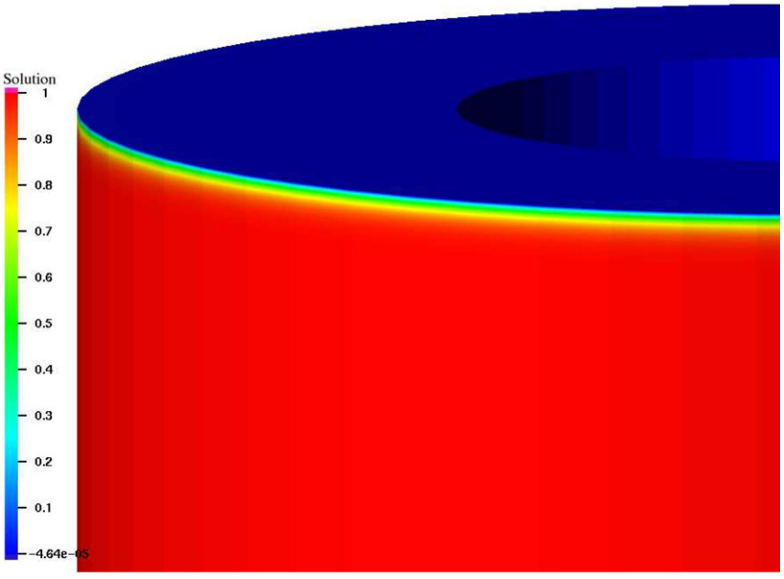

Detail of the outflow boundary layer

Fig. 7. Advection–diffusion in an annular region. Solution contours on the finest mesh.

and

$$(\boldsymbol{W},\boldsymbol{F}) = (\boldsymbol{w},\boldsymbol{f})_{\Omega}. \tag{28}$$

The Euler–Lagrange equations of this formulation are the momentum equations and the incompressibility constraint. We approximate Eqs. (26)–(28) by the following variational problem over the finite element spaces:

Find $\boldsymbol{U}^h = \{\boldsymbol{u}^h, p^h\} \in \mathscr{V}^h$, $\boldsymbol{u}^h \cdot \boldsymbol{n} = 0$ on Γ such that $\forall \boldsymbol{W}^h = \{\boldsymbol{w}^h, q^h\} \in \mathscr{V}^h$, $\boldsymbol{w}^h \cdot \boldsymbol{n} = 0$ on Γ,

$$\begin{aligned}
&\left(\boldsymbol{w}^h, \frac{\partial \boldsymbol{u}^h}{\partial t}\right)_{\Omega} - (\nabla \boldsymbol{w}^h, \boldsymbol{u}^h \otimes \boldsymbol{u}^h)_{\Omega} + (q^h, \nabla \cdot \boldsymbol{u}^h)_{\Omega} \\
&\quad - (\nabla \cdot \boldsymbol{w}^h, p^h)_{\Omega} + (\nabla^s \boldsymbol{w}^h, 2\nu \nabla^s \boldsymbol{u}^h)_{\Omega} - (\boldsymbol{w}^h, \boldsymbol{f})_{\Omega} \\
&\quad + \sum_{e=1}^{n_{el}} (\mathbb{L}\boldsymbol{W}^h \boldsymbol{\tau}, \mathfrak{Q}\boldsymbol{U}^h - \boldsymbol{F})_{\Omega_e} - \sum_{b=1}^{n_{eb}} (\boldsymbol{w}^h, 2\nu \nabla^s \boldsymbol{u}^h \cdot \boldsymbol{n})_{\Gamma_b \cap \Gamma} \\
&\quad - \sum_{b=1}^{n_{eb}} (\gamma 2\nu \nabla^s \boldsymbol{w}^h \cdot \boldsymbol{n}, \boldsymbol{u}^h - \boldsymbol{0})_{\Gamma_b \cap \Gamma} \\
&\quad + \sum_{b=1}^{n_{eb}} \left(\boldsymbol{w}^h \frac{C_b^I \nu}{h_b}, \boldsymbol{u}^h - \boldsymbol{0}\right)_{\Gamma_b \cap \Gamma} = 0.
\end{aligned} \tag{29}$$

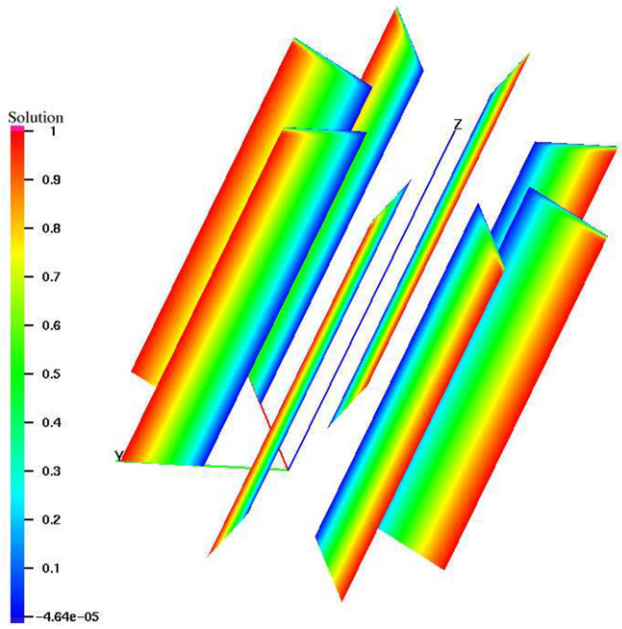

Fig. 8. Advection–diffusion in an annular region. Solution contours on the finest mesh. Axisymmetry is evident from the contours at various angular positions.

In the numerical calculations we used the stabilized formulation of Tejada-Martinez and Jansen [47] in which

$$(\mathbb{L}\boldsymbol{W}^h\boldsymbol{\tau}, \mathfrak{L}\boldsymbol{U}^h - \boldsymbol{F})_{\Omega_e} = (\{\boldsymbol{u}^h \cdot \nabla \boldsymbol{w}^h + \boldsymbol{u}^h \cdot (\nabla \boldsymbol{w}^h)^{\mathrm{T}} + \nabla q^h\}\tau_M, \mathscr{L}\boldsymbol{U}^h - \boldsymbol{f})_{\Omega_e} + (\nabla \cdot \boldsymbol{w}^h \tau_C, \nabla \cdot \boldsymbol{u}^h)_{\Omega_e}, \tag{30}$$

$$\mathfrak{L}\boldsymbol{U}^h = \begin{Bmatrix} \mathscr{L}\boldsymbol{U}^h \\ \nabla \cdot \boldsymbol{u}^h \end{Bmatrix} \tag{31}$$

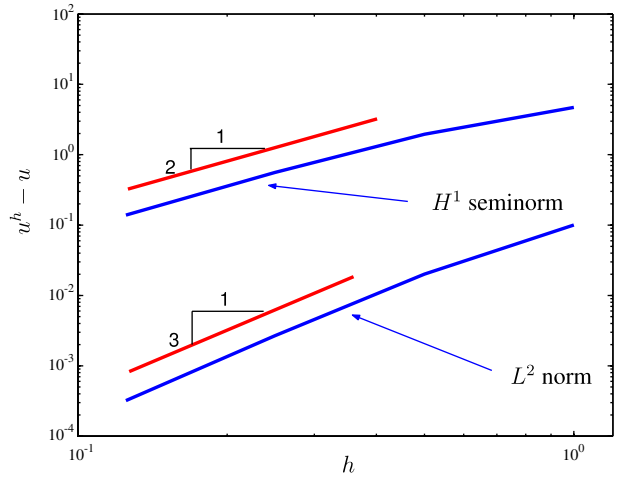

Fig. 10. Advection–diffusion in an annular region. Convergence to the exact solution.

and

$$\mathscr{L}\boldsymbol{U}^h = \frac{\partial \boldsymbol{u}^h}{\partial t} + \nabla \cdot (\boldsymbol{u}^h \otimes \boldsymbol{u}^h) + \nabla p^h - \nabla \cdot 2\nu\nabla^s \boldsymbol{u}^h. \tag{32}$$

Remarks

(1) For further details of stabilized formulations of INS, see Taylor et al. [46] and Jansen et al. [36]. In particular, these references may be consulted for definitions of τ_M and τ_C.

(2) We chose to enforce the normal component (i.e., no-penetration condition) of the no-slip boundary condition strongly on the trial and the weighting spaces.

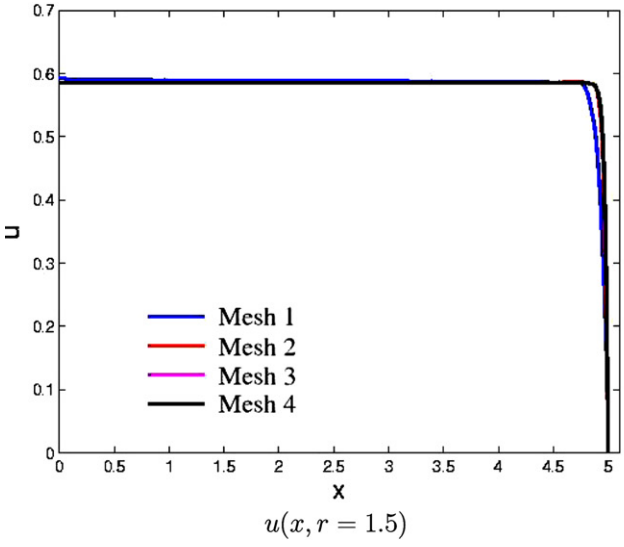

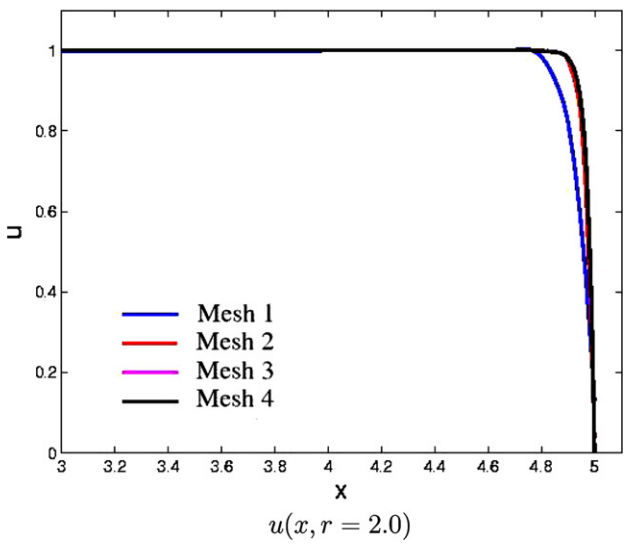

Fig. 9. Advection–diffusion in an annular region. Line plots of solution as a function of the axial coordinate at two radial positions. Solutions are monotone and the boundary conditions are well approximated.

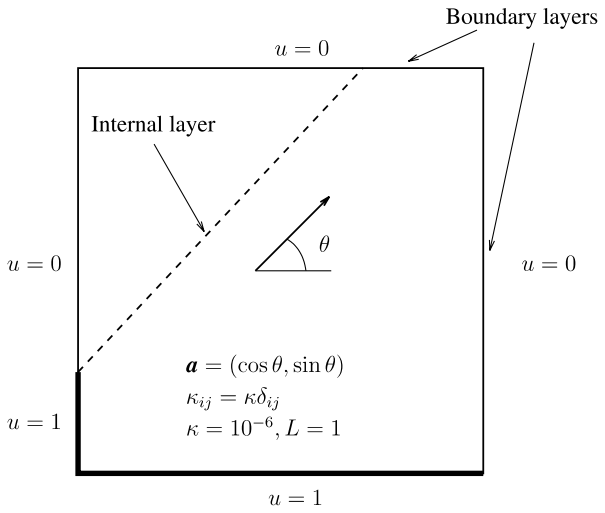

Fig. 11. Advection skew to mesh. Problem description and data.

(3) The third from last term of (29) is the consistency term. Notice that the no-penetration condition on the trial and the weighting spaces leaves only a viscous contribution in this term.
(4) The last two terms of (29) are responsible for the enforcement of the Dirichlet boundary conditions on the remaining components of the velocity vector. The construction of these terms was motivated in the section on the advection–diffusion equation. The constants γ and C_b^I retain their previous meaning.

4.1. Turbulent channel flow at $Re_\tau = 180$

Formulation (29) was tested on the $Re_\tau = 180$ turbulent channel flow (see Kim et al. [37]) and compared

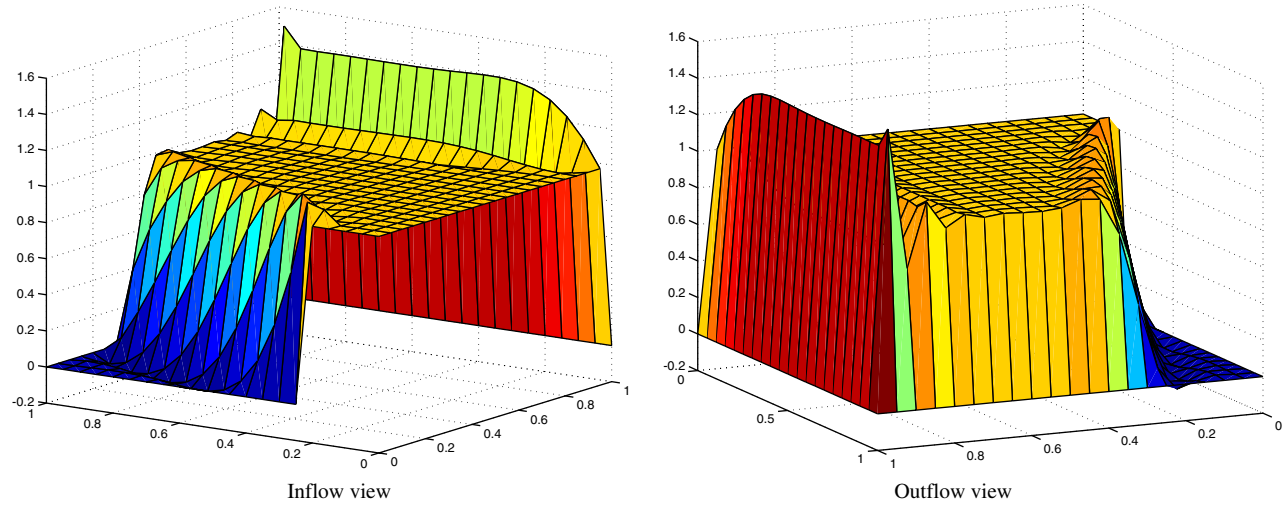

Fig. 12. Advection skew to the mesh. All strong Dirichlet boundary conditions.

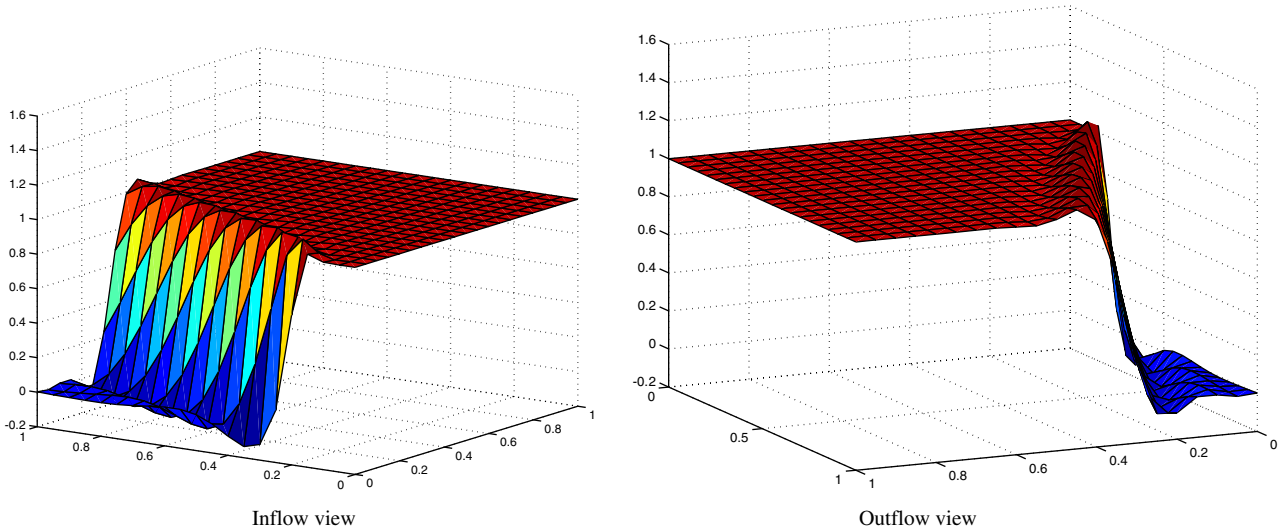

Fig. 13. Advection skew to the mesh. All weak Dirichlet boundary conditions.

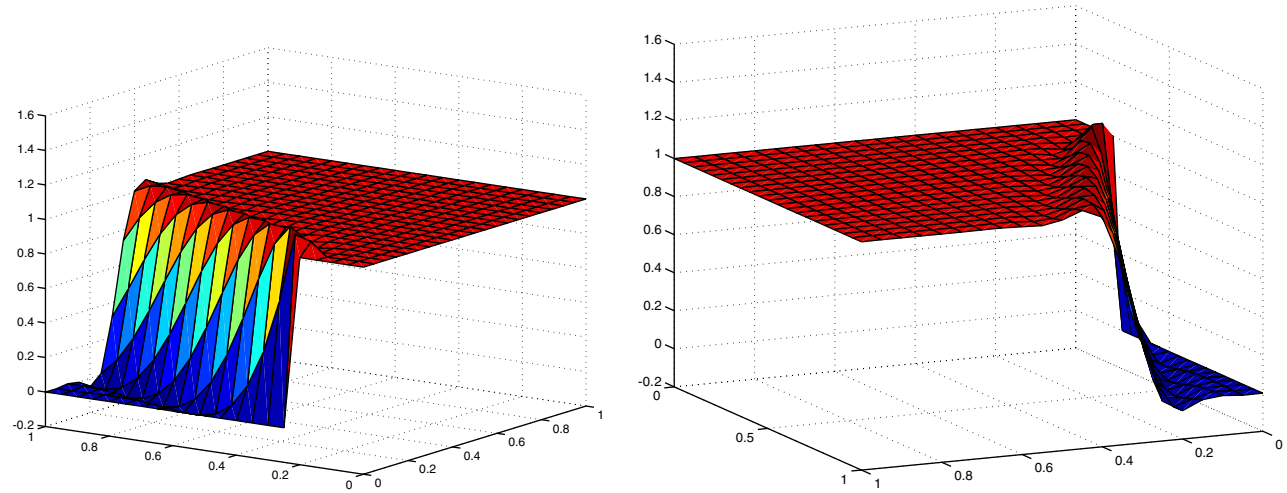

Fig. 14. Advection skew to the mesh. Strong inflow–weak outflow Dirichlet BC solution.

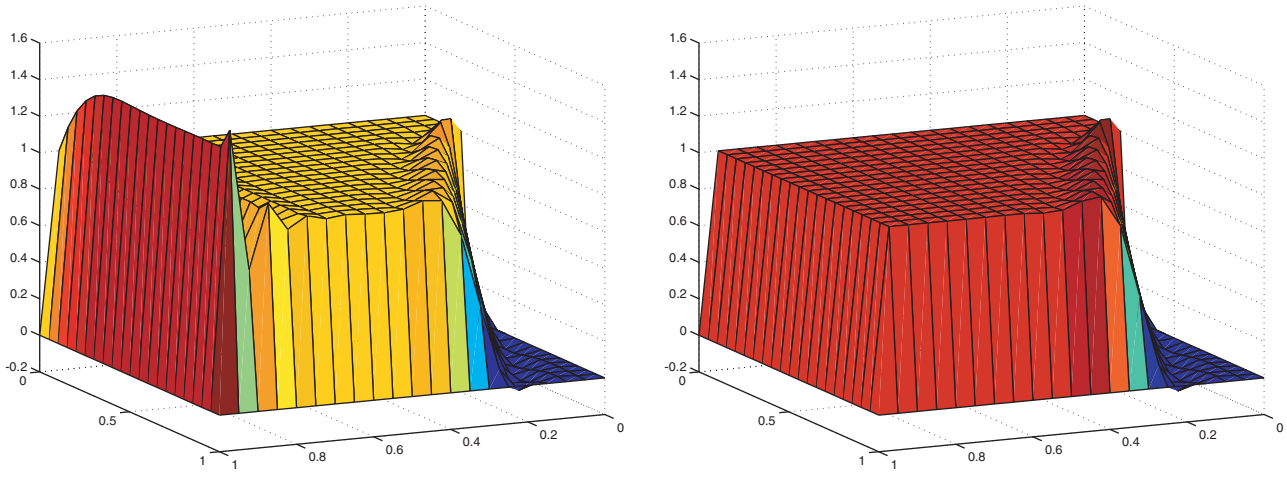

Fig. 15. Advection skew to the mesh. Comparison of all strong and strong inflow–weak outflow solutions. The latter was postprocessed to account for the prescribed Dirichlet boundary conditions, a technique often employed in commercial finite volume codes [52].

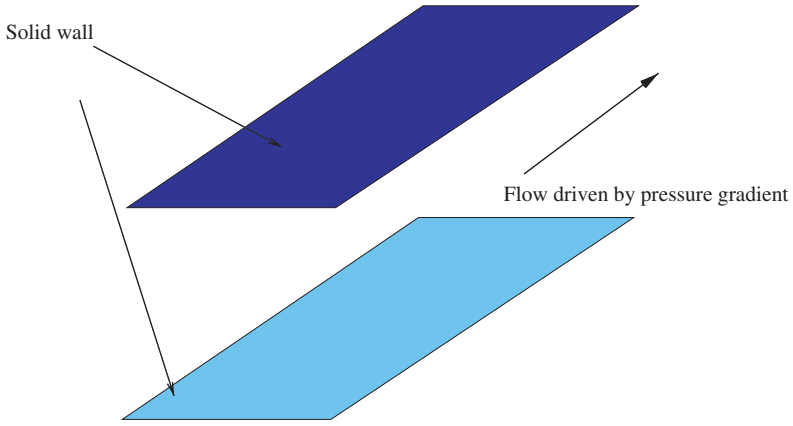

Fig. 16. Turbulent channel flow. Problem setup.

with the strong imposition of the no-slip condition. In the case when the no-slip condition is imposed strongly, the last three terms of (29) vanish yielding a standard stabilized method for INS. The domain size is 4π, 2, and $4/3\pi$ in the stream-wise, wall-normal, and span-wise directions, respectively. Periodic boundary conditions are imposed in the stream-wise and span-wise directions, while a homogeneous Dirichlet boundary condition is set in the wall-normal direction. Fig. 16 shows the schematic of the computational setup. Uniform meshes of $8 \times 16 \times 8$, $16 \times 32 \times 16$, and $32 \times 64 \times 32$ trilinear finite elements were used in the computation. The discrete equations were advanced in time using the Generalized-α method (see Chung and Hulbert [16] for details). The adjoint-consistent ($\gamma = 1$) form was used in the case of weak boundary conditions. C_b^I was set equal to 4. Fig. 17 shows the stream-wise velocity contours at an instant in time for the finest simulation employing weak boundary conditions. Note the presence of turbulent structures on the no-slip wall.

Mean flow statistics were computed by averaging the solution in time as well as in the homogeneous directions, namely stream-wise and span-wise. Fig. 18a shows convergence of the mean flow to the reference DNS computation of Kim, Moin, and Moser [37] for the case of strongly enforced boundary conditions. The coarsest mesh gives a significant over-prediction of the mean flow, the medium mesh gives a better result, yet the solution is still noticeably in error compared with the benchmark, while the finest mesh, which is still significantly coarser than the DNS resolution, gives a result very close to it. The same quantity was computed and plotted for the weak boundary condition formulation (see

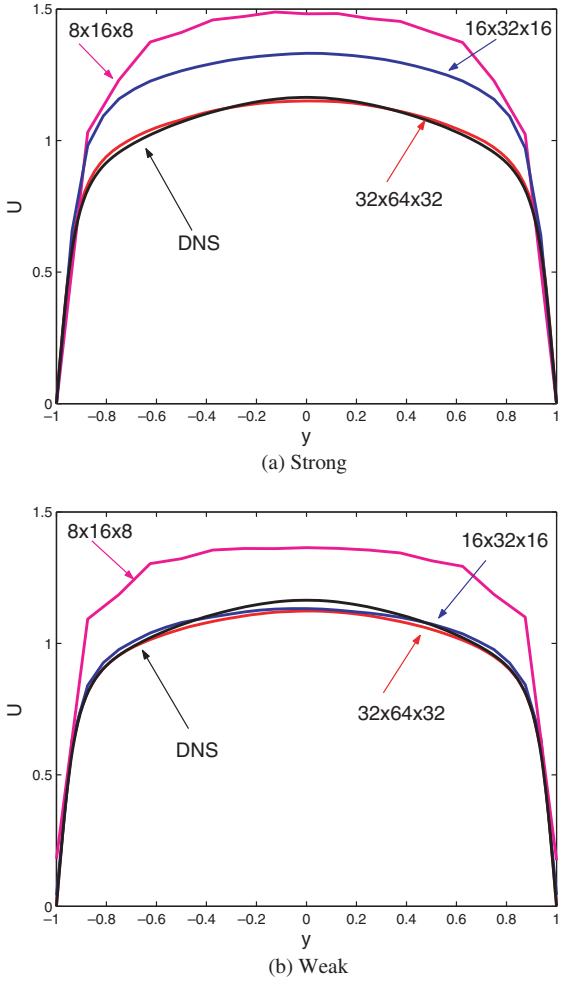

Fig. 18. Turbulent channel flow. Convergence of the mean flow. Comparison between weak and strong imposition of the no-slip boundary condition.

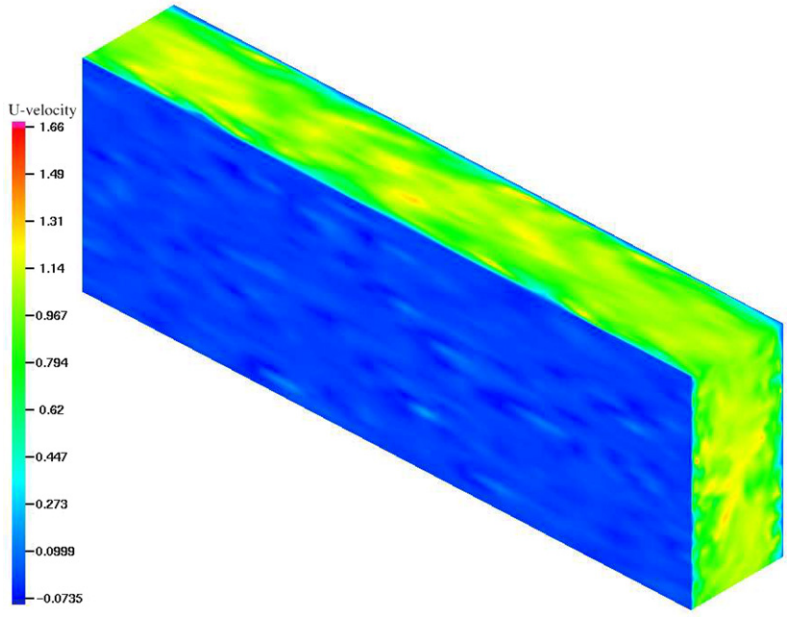

Fig. 17. Turbulent channel flow. Stream-wise velocity contours.

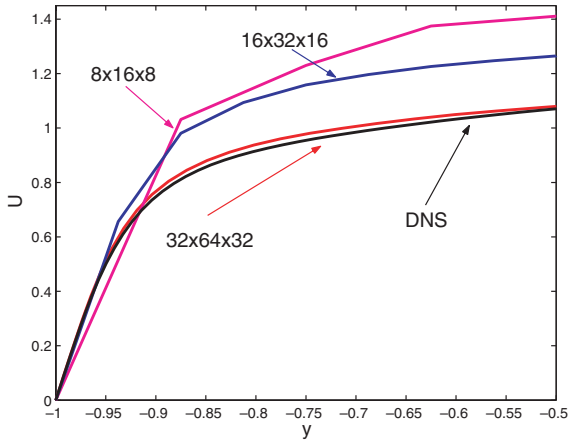

(a) Strong

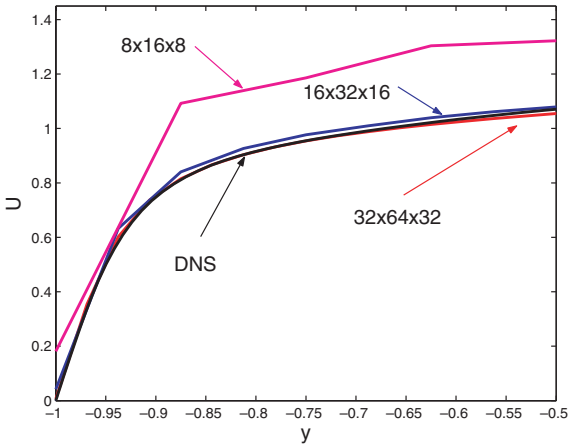

(b) Weak

Fig. 19. Turbulent channel flow. Convergence of the mean flow in the boundary layer. Comparison between weak and strong imposition of the no-slip boundary condition.

Fig. 18b). The mean flow is still over-predicted on the coarsest mesh but the result is closer to the DNS than its strong counterpart. The medium mesh result is remarkable in that the mean flow is in very close agreement with the DNS, and much better than the corresponding strong boundary condition computation. The fine mesh results are almost identical to the medium mesh results.

Some deviation is seen in the core of the channel for all methods presented here. One needs to keep in mind that formulation (29) is not a bona fide turbulence model, although the stabilization terms represent a model of the cross-stress terms. Consequently, the calculations may be thought of as being somewhere between a coarse DNS and LES. Presumably, a variational multiscale LES formulation would lead to better results (see Hughes et al. [30], Hughes et al. [27], Hughes et al. [28], Hughes et al. [29], Holmen et al. [25], Hughes et al. [35], Hughes et al. [31], and Calo [14]). Fig. 19 shows results in the boundary layer region. Weak boundary condition calculations appear to be much more accurate on coarse meshes than their strong counterparts.

5. Conclusions

We have developed stabilized formulations of the advection–diffusion and incompressible Navier–Stokes equations incorporating weak enforcement of Dirichlet boundary conditions. In the case of the Navier–Stokes equations, this amounts to the weak treatment of the no-slip condition. We compared weakly and strongly enforced Dirichlet boundary conditions on problems involving unresolved boundary layers and we found weak treatment to be superior to strong. In the case of a turbulent channel flow, weak treatment seemed to behave like a wall function although the design of the boundary condition was based on numerical considerations rather than physical or empirical turbulence concepts. Convergence of the mean flow was much more rapid in the weakly enforced case than in the strongly enforced case. These results are intriguing and warrant further investigation.

We believe our study has provided some interesting and practically useful results. However, it has only scratched the surface of the topic. In order to more fully understand the behavior of weak treatment of Dirichlet conditions we need to evaluate the conservative formulation for the calculation of diffusive flux derived herein but not yet tested. Furthermore, to fully assess the possibilities in turbulence simulations, a bona fide LES turbulence model should be tested. Our intent is to utilize residual-based models based on the variational multiscale formulation for this purpose. In addition to mean flow quantities, we also need to study higher-order statistics.

References

[1] Abedi P, Patracovici B, Haber RB. A spacetime discontinuous Galerkin method for linearized elastodynamics with element-wise momentum balance. Comput Methods Appl Mech Eng, in press.
[2] Adjerid S, Massey TC. Superconvergence of discontinuous Galerkin solutions for a nonlinear scalar hyperbolic problem. Comput Methods Appl Mech Eng, in press.
[3] Akin JE, Tezduyar TE. Calculation of the advective limit of the SUPG stabilization parameter for linear and higher-order elements. Comput Methods Appl Mech Eng 2004;193:1909–22.
[4] Antonietti PF, Buffa A, Perugia I. Discontinuous Galerkin approximation of the Laplace eigenproblem. Comput Methods Appl Mech Eng, in press.
[5] Arnold DN, Brezzi F, Cockburn B, Marini LD. Unified analysis of Discontinuous Galerkin methods for elliptic problems. SIAM J Numer Anal 2002;39:1749–79.
[6] Barth T. On discontinuous Galerkin approximations of Boltzmann moment systems with levermore closure. Comput Methods Appl Mech Eng, in press.

[7] Baumann CE, Oden JT. A discontinuous hp finite element method for convection–diffusion problems. Comput Methods Appl Mech Eng 1999;175:311–41.
[8] Bischoff M, Bletzinger K-U. Improving stability and accuracy of Reissner–Mindlin plate finite elements via algebraic subgrid scale stabilization. Comput Methods Appl Mech Eng 2004;193:1491–516.
[9] Bochev PB, Gunzburger MD, Shadid JN. On inf–sup stabilized finite element methods for transient problems. Comput Methods Appl Mech Eng 2004;193:1471–89.
[10] Brezzi F, Cockburn B, Marini LD, Suli E. Stabilization mechanisms in discontinuous Galerkin finite element methods. Comput Methods Appl Mech Eng, in press.
[11] Brezzi F, Hughes TJR, Süli E. Variational approximation of flux in conforming finite element methods for elliptic partial differential equations: a model problem. Rend Mat Acc Lincei 2002;9:167–83.
[12] Brooks AN, Hughes TJR. Streamline upwind/Petrov–Galerkin formulations for convection dominated flows with particular emphasis on the incompressible Navier–Stokes equations. Comput Methods Appl Mech Eng 1982;32:199–259.
[13] Burman E, Hansbo P. Edge stabilization for Galerkin approximations of convection–diffusion-reaction problems. Comput Methods Appl Mech Eng 2004;193:1437–53.
[14] Calo VM. Residual-based multiscale turbulence modeling: finite volume simulation of bypass transition. PhD thesis, Department of Civil and Environmental Engineering, Stanford University, 2004.
[15] Chinosi C, Lovadina C, Marini LD. Nonconforming locking-free finite elements for Reissner–Mindlin plates. Comput Methods Appl Mech Eng, in press.
[16] Chung J, Hulbert GM. A time integration algorithm for structural dynamics with improved numerical dissipation: the generalized-α method. J Appl Mech 1993;60:371–5.
[17] Ciarlet PG. The finite element method for elliptic problems. Amsterdam: North-Holland; 1978.
[18] Cockburn B, Schotzau D, Wang J. Discontinuous Galerkin methods for incompressible elastic materials. Comput Methods Appl Mech Eng, in press.
[19] Codina R, Soto O. Approximation of the incompressible Navier–Stokes equations using orthogonal subscale stabilization and pressure segregation on anisotropic finite element meshes. Comput Methods Appl Mech Eng 2004;193:1403–19.
[20] Coutinho ALGA, Diaz CM, Alvez JLD, Landau L, Loula AFD, Malta SMC, et al. Stabilized methods and post-processing techniques for miscible displacements. Comput Methods Appl Mech Eng 2004;193:1421–36.
[21] Gravemeier V, Wall WA, Ramm E. A three-level finite element method for the instationary incompressible Navier–Stokes equations. Comput Methods Appl Mech Eng 2004;193:1323–66.
[22] Grooss J, Hesthaven JS. A level-set discontinuous Galerkin method for free-surface flows. Comput Methods Appl Mech Eng, in press.
[23] Harari I. Stability of semidiscrete formulations for parabolic problems at small time steps. Comput Methods Appl Mech Eng 2004;193:1491–516.
[24] Hauke G, Valiño L. Computing reactive flows with a field Monte Carlo formulation and multi-scale methods. Comput Methods Appl Mech Eng 2004;193:1455–70.
[25] Holmen J, Hughes TJR, Oberai AA, Wells GN. Sensitivity of the scale partition for variational multiscale LES of channel flow. Phys Fluids 2004;16(3):824–7.
[26] Houston P, Schotzau D, Wihler TP. An *hp*-adaptive mixed discontinuous Galerkin FEM for nearly incompressible linear elasticity. Comput Methods Appl Mech Eng, in press.
[27] Hughes TJR, Mazzei L, Jansen KE. Large-eddy simulation and the variational multiscale method. Comput Visual Sci 2000;3:47–59.
[28] Hughes TJR, Mazzei L, Oberai AA, Wray AA. The multiscale formulation of large eddy simulation: decay of homogenous isotropic turbulence. Phys Fluids 2001;13(2):505–12.
[29] Hughes TJR, Oberai AA, Mazzei L. Large-eddy simulation of turbulent channel flows by the variational multiscale method. Phys Fluids 2001;13(6):1784–99.
[30] Hughes TJR, Scovazzi G, Franca LP. Multiscale and stabilized methods. In: Stein E, De Borst R, Hughes TJR, editors. Encyclopedia of computational mechanics. Computational fluid dynamics, vol. 3. Wiley; 2004 [Chapter 2].
[31] Hughes TJR, Calo VM, Scovazzi G. Variational and multiscale methods in turbulence. In: Gutkowski W, Kowalewski TA, editors. Proceedings of the XXI international congress of theoretical and applied mechanics (IUTAM). Kluwer; 2004.
[32] Hughes TJR, Cottrell JA, Bazilevs Y. Isogeometric analysis: CAD, finite elements, NURBS, exact geometry, and mesh refinement. Comput Methods Appl Mech Eng 2005;194:4135–95.
[33] Hughes TJR, Engel G, Mazzei L, Larson M. The continuous Galerkin method is locally conservative. J Computat Phys 2000;163(2):467–88.
[34] Hughes TJR, Masud A, Wan J. A stabilized mixed discontinuous Galerkin method for Darcy flow. Comput Methods Appl Mech Eng, in press.
[35] Hughes TJR, Wells GN, Wray AA. Energy transfers and spectral eddy viscosity of homogeneous isotropic turbulence: comparison of dynamic Smagorinsky and multiscale models over a range of discretizations. Technical report, ICES, The University of Texas at Austin, 2004.
[36] Jansen KE, Whiting CH, Hulbert GM. A generalized-α method for integrating the filtered Navier–Stokes equations with a stabilized finite element method. Comput Methods Appl Mech Eng 1999;190:305–19.
[37] Kim J, Moin P, Moser R. Turbulence statistics in fully developed channel flow at low Reynolds number. J Fluid Mech 1987;177:133.
[38] Koobus B, Farhat C. A variational multiscale method for the large eddy simulation of compressible turbulent flows on unstructured meshes—application to vortex shedding. Comput Methods Appl Mech Eng 2004;193:1367–83.
[39] Layton W. Weak imposition of "no-slip" boundary conditions in finite element methods. Comput Math Appl 1999;38:129–42.
[40] Lin G, Karniadakis G. A discontinuous Galerkin method for two-temperature plazmas. Comput Methods Appl Mech Eng, in press.
[41] Masud A, Khurram RA. A multiscale/stabilized finite element method for the advection–diffusion equation. Comput Methods Appl Mech Eng 2004;193:1997–2018.
[42] Riviere B, Girault V. Discontinuous finite element methods for incompressible flows on subdomains with non-matching interfaces. Comput Methods Appl Mech Eng, in press.
[43] Riviere B, Wheeler MF, Girault V. A priori error estimates for finite element methods based on discontinuous approximation spaces for elliptic problems. SIAM J Numer Anal 2001;39(3):902–31.
[44] Romkes A, Prudhomme S, Oden JT. Convergence analysis of a discontinuous finite element formulation based on second order derivatives. Comput Methods Appl Mech Eng, in press.
[45] Sun S, Wheeler MF. Anisotropic and dynamic mesh adaptation for discontinuous Galerkin methods applied to reactive transport. Comput Methods Appl Mech Eng, in press.
[46] Taylor CA, Hughes TJR, Zarins CK. Finite element modeling of blood flow in arteries. Comput Methods Appl Mech Eng 1998;158:155–96.

[47] Tejada-Martinez AE, Jansen KE. On the interaction between dynamic model dissipation and numerical dissipation due to streamline upwind/Petrov–Galerkin stabilization. Comput Methods Appl Mech Eng 2005;194:1225–48.
[48] Tezduyar TE, Sathe S. Enhanced-discretization space-time technique (EDSTT). Comput Methods Appl Mech Eng 2004;193:1385–401.
[49] Tezduyar TE. Computation of moving boundaries and interfaces and stabilization parameters. Int J Numer Methods Fluids 2003;43:555–75.
[50] Warburton T, Embree M. The role of the penalty in the local discontinuous Galerkin method for Maxwell's eigenvalue problem. Comput Methods Appl Mech Eng, in press.
[51] Wheeler MF. An elliptic collocation-finite element method with interior penalties. SIAM J Numer Anal 1978;15:152–61.
[52] Xu W. Private communication.
[53] Xu Y, Shu C-W. Local discontinuous Galerkin methods for the Kuramoto-Sivashinsky equations and the Ito-type coupled KdV equations. Comput Methods Appl Mech Eng, in press.